IMPORTANT NOTE : Please be aware that slight modifications occurring after Proof correction may occur between this version of the manuscript and the version on the Publisher's website----------

pH-triggered formation of nanoribbons from yeast-derived glycolipid biosurfactants

Authors

Anne-Sophie Cuvier,[1],[2],[3] Jan Berton,[4] Chris Stevens,[4] Giulia C. Fadda,[5] Florence Babonneau,[1],[2],[3] Inge N. A. Van Bogaert,[6] Wim Soetaert,[6] Gérard Pehau-Arnaudet,[7] Niki Baccile*[1],[2],[3]

Affiliations

[1] UPMC Univ Paris 06, UMR 7574, Chimie de la Matière Condensée de Paris, F-75005, Paris, France. E-mail : niki.baccile@upmc.fr

[2] CNRS, UMR 7574, Chimie de la Matière Condensée de Paris, F-75005, Paris, France

[3] Collège de France, UMR 7574, Chimie de la Matière Condensée de Paris, F-75005, Paris, France

[4] SynBioC Research Group, Departement of Sustainable Organic Chemistry and Technology, Faculty of Bioscience Engineering, Ghent University, Coupure links 653, B-9000 Gent, Belgium

[5] Laboratoire Léon Brillouin, LLB, CEA Saclay, F-91191 Gif-sur-Yvette Cedex, France

[6] InBio, Department of Biochemical and Microbial Technology, Faculty of Bioscience Engineering, Ghent University, Coupure Links 653, 9000, Ghent, Belgium

[7] Institut Pasteur, UMR3528, 28 Rue du Docteur Roux, F-75015, Paris, France

Abstract

Supramolecular chirality which is an important phenomenon at the basis of life but also in proteins and lipids, is still poorly understood and difficult to predict although it is very interesting for applications like hydrogelation, templates for mineral supports for enantiomeric separations andtissue engineering. In the present paper, we show that the saturated form of sophorolipids, a family of industrially-scaled bolaform glycolipid biosurfactants, unexpectedly form chiral nanofibers only under neutral and acidic pH conditions. In particular, we illustrate that this phenomenon derives from a subtile cooperative effect of molecular chirality, hydrogen bonding, van der Waals forces and steric hindrance. The pH-responsive behaviour was shown by Dynamic Light Scattering (DLS), pH-titration and Field Emission Scanning Electron Microscopy (FE-SEM) while the nanoscale chirality was put in evidence with Circular Dichroism (CD) and cryo Transmission Electron Microscopy (cryo-TEM). The packing of sophorolipids within the ribbons was studied using Small Angle Neutron Scattering (SANS), Wide Angle X-ray Scattering (WAXS) and 2D ^{1}H-^{1}H through-space correlations via Nuclear Magnetic Resonance under very fast (67 kHz) Magic Angle Spinning (MAS-NMR).

Introduction

Supramolecular self-assembly of natural and synthetic amphiphiles is an important topic in nanoscience, as it constitutes a promising tool to build complex 1D to 3D nanoscale objects.[1] In particular, the effect of chirality on supramolecular self-assembly is at the origin of life (DNA), but also of tissue and bone engineering (collagen), of a number of human diseases including various neurodegenerative disorders (amyloid fibrillation), but also structural protection of microorganisms (capsid formation in viruses). Chirality-induced structural strength, mechanical rigidity and functionality[2,3] strongly impact the properties and role of self-assembled soft systems (proteins, lipids, nucleic acids) in natural processes.[4,5] A seminal example is constituted by collagen forming a triple helix and for which its improved mechanical properties strongly depend on its intrinsic chirality.[6] More recently, bioinspired synthetic compounds that combine 1D assembly and functionality started to be explored. The group of Stupp has shown the potential of synthetic peptide amphiphiles, reported to form nanoscale fibers, tubes and chiral ribbons[7–10] and used

them in medical applications to promote bioactivity like spinal cord, bone and cartilage regeneration.[11–13]

Other compounds like simple peptides, alkylammonium surfactants, alkylglycosides or aminoacid-based amphiphiles can be used to form chiral fibers by controlling their chemical (type of amino acid,[14] linker between sugars, hydrophobic moiety[15]) and/or physico-chemical (counterion[16] pH[17,18]) properties. The range of applications is very broad: encapsulation of biomolecules, drug release, cell adhesion, antimicrobial activity, tissue engineering, nanoreactors, nanoelectronics, wound healing, hydrogelation, scaffolding and templates for nanowires, nanoparticles and mineralization.[19–29]

The mechanisms leading to chiral structures have been matter of intense research. Initial theoretical studies date from the late 1980's, early 1990's,[30–32] but the general rationale describing the morphological evolution of micelles to twisted and helical ribbons, and finally to nanotubes has only recently started to be unraveled by combining a variety of experimental, theoretical and structural approaches.[33–36,14] Despite such an important amount of research, it is still nowadays impossible to predict in advance the type of assembly that a given amphiphile will form and under which conditions this will occur. Even if it is generally admitted that stereocenter(s) can promote the formation of 1D chiral superstructures, several examples illustrate that this parameter alone is either not sufficient or even not necessary. This was shown for a racemic mixture of D- and L-alanine derived amphiphiles, which exclusively form macroscopic left-handed twisted ribbons,[37] while for racemates a mixture of left- and right-handed twists should be expected.[38,37]

In this context, glycolipids constitute an important class of amphiphiles that are generally obtained from bio-derived building blocks (sugars and fatty acids, or fatty alcohols).[39] Thus, they are gaining more and more interest because of their biocompatibility, biodegradability and low toxicity. In particular, the use of sugars is of specific interest because of their biologically-relevant functionality[40,41] occurring in cell-cell agglutination mechanisms, but new nanotech-based applications are also being explored.[42,24] Among this class of compounds, sophorolipids, natural bolaform glycolipids, can be obtained from the fermentation process of the yeast *Starmerella bombicola* (Figure 1a) and are the best bioderived candidates to substitute their synthetic counterparts previously studied,[43,44] both in terms of properties and conditions of productions.[45,46]

Even if predictions cannot be done, it has been empirically observed that fibers with nanoscale chirality can be formed in glycolipid-based systems if specific sugar-to-lipid linkers like phenyl,[15] phenylamide[47] or amidopyridine[48] groups are used over simple ether bonding.[15] The former enhance hydrogen bonding[47,49,35] or π–π stacking whereas the latest only promote the formation of micelles. Asymmetric synthetic glycolipids (glucose and COOH headgroups) were mainly reported to form nanotubes.[24] In the case of sophorolipids, nanoscale chirality has never been reported even if giant ribbons seem to be formed from an elaidic acid (C18:1-*trans*) based compound while contradictory results exists (giant ribbons *versus* micelles) on the behavior of oleic acid derived (C18:1-*cis*) sophorolipids.[50,51,52,53]

In the present paper, we present the pH-triggered formation of self-assembled fibers with nanoscale chirality using a saturated sophorolipid (C18:0 sophorolipids, Figure 1b) thus contributing to the development of interesting pH-responsive bio-based chiral materials. We highlight the fact that acidic C18:0 sophorolipids contain all those chemical elements (ether bond junction, headgroups asymmetry) that have shown to provide the least chiral activity:[15,46,54] this same compound was reported to form flat sheets by Prabhu and co.[51] For this reason, this work provides additional arguments to the general problem of chirality prediction and control in lipid-based systems.

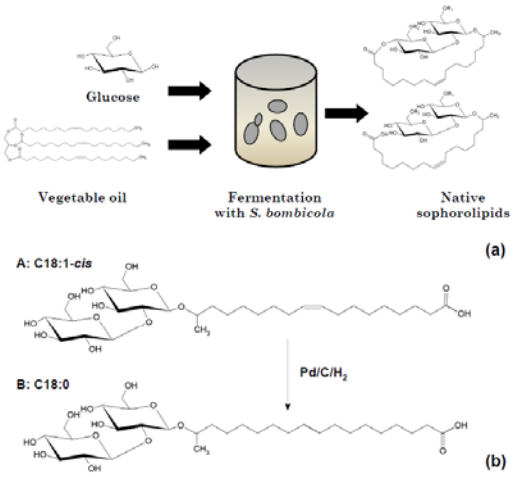

Figure 1 : (a) Scheme showing the synthesis process of native sophorolipids using the yeast *Starmerella bombicola*. (b) Reaction scheme of the hydrogenation of the acidic C18:1-*cis* sophorolipids (A) to obtain the saturated C18:0 sophorolipids (B)

Experimental

The detailed synthesis of sophorolipids can be found in *section S.1* in the Supplementary Information.

Purity by NMR and chromatography: The ^{1}H spectrum of C18:1-*cis* and C18:0 sophorolipids are shown and described in *section S.2* (*Figure S1 a, b*). In particular, the $CH_{9,10}$ signal of the C<u>H</u>=C<u>H</u> group in the C18:1-*cis* at δ = 5.17 - 5.32 ppm has disappeared in the C18:0 sample as well as the signal of the allylic C<u>H</u>$_{8,11}$ positions. The typical signature of an aliphatic end-of-chain R-$CH_2C\underline{H}_3$ methyl at δ < 0.95 ppm, indicating the presence of possible, residual, fatty acids is not detected, thus proving the purity of the compound. This is confirmed by HPLC analysis (*section S.3*, *Figure S2 a, b)* showing that the samples consist of > 95% unacetylated acidic C18:1-*cis* and C18:0 sophorolipids, respectively. LC-MS (results not shown) is used to confirm that the molar mass for C18:1-*cis* sophorolipids is 622 g/mol. The other compounds in the mixture only differ in the nature of the lipid moiety, which is typical for this particular microbial synthesis.

Preparation of the supramolecular assemblies: Different amounts of acidic C18:0 sophorolipids (c= 2 mg/mL and 5 mg/mL) were solubilized in deionized water. Due to the poor solubility of the C18:0 sophorolipids, pH was first increased to 11 using a 1 M NaOH solution and then decreased to pH= 2 and 6 with µmolar amounts of 0.5 and 0.05 M HCl solutions respectively. pH measurements were done with a classical pH-meter. All samples were freshly prepared and characterized right after their preparation. Additionally, a freshly prepared solution (1 mL) of 5 mg/mL C18:0 SL whose pH was adjusted to 3.2 was dialyzed against deionized water for 3 days to remove sodium chloride using a cellulose membrane with a molecular-weight cutoff of 3.500.

Characterization techniques

Please refer to the Supplementary Information section (*section S.4*).

Results and discussion

The C18:0 sophorolipids are studied here at concentrations as high as 5 mg/mL after a previous solubilization step at pH= 11, from where the pH-dependent light diffusion properties are then explored using Dynamic Light Scattering (DLS), as shown in Figure 2.

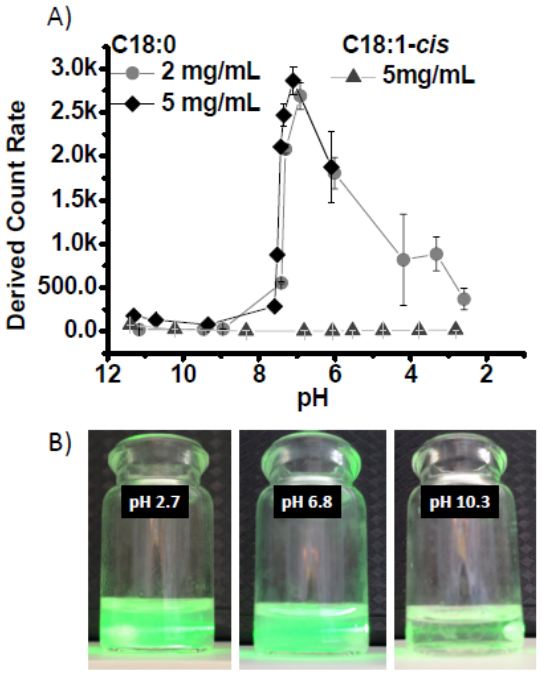

Figure 2 - A: pH-dependent light scattering for C18:0 and C18:1-*cis* sophorolipids solutions. B: Visual effect of the light diffusion property for the C18:0 sophorolipids with pH

At pH values above 9, a clear solution is formed that becomes more and more opaque when decreasing the pH below 8, as shown in Figure 2B. This phenomenon is observed by DLS measuring the amount of light scattered, at a constant shutter opening. For the C18:0 sophorolipids, independently of the initial concentration, the diffused light increases from an average of $<10^1$ kcps at pH= 11.2 to $>10^3$ kcps at pH=

6.9 (Figure 2A). Upon further acidification to about pH= 2, the value of the scattered light's intensity slightly diminishes, while the solution remains highly turbid. Similar effects are observed for the 5 mg/mL solution. For comparison purposes, Figure 2A also reports the light scattering properties of a C18:1-*cis* sophorolipids solution at 5 mg/mL, whose pH-dependent self-assembly in water has been previously studied.[52,53] Clearly, if compared to its hydrogenated counterpart, the C18:1-*cis* sophorolipids do not experience the same intense light scattering phenomenon upon the equivalent pH cycle, thus showing the strong influence of unsaturation on the self-assembly. This aspect will be detailed in the discussion section. To eliminate the possibility that this light scattering phenomenon is related to the presence of salt (NaCl) upon lowering the pH, we confirmed that light scattering also occurs on a dialyzed solution of C18:0 sophorolipids at pH= 3.2 (results not shown): pH is the only parameter affecting the assembly of C18:0 sophorolipids.

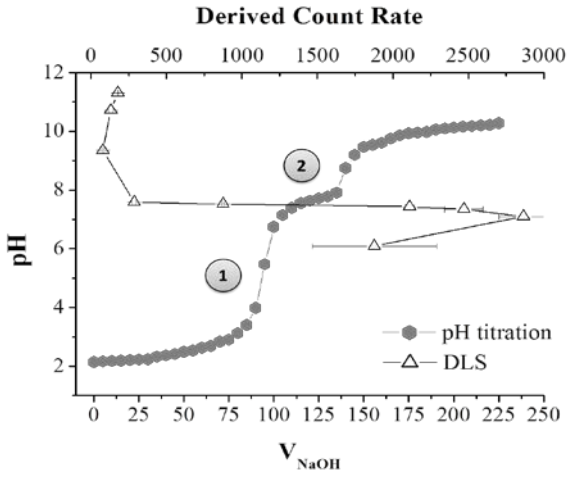

Figure 3 - Titration curve performed at 25°C on the C18:0 sophorolipids (5 mg/mL). The DLS light scattering data for the same sample is also shown (empty triangles)

The pH titration curve of the C18:0 sophorolipids in water is shown in Figure 3 while the detailed calculations are discussed in *Section S.5*.

The equivalent point 1 in Figure 3 corresponds to the titration of HCl in solution. The pH at the equivalence is pH(V_{eq1})= 5.2, which depends on the soluble fraction of C18:0 sophorolipids (see also Eq.S2), estimated at 10^{-6} M. If compared to the initial concentration of C18:0 sophorolipids, $1.6 \cdot 10^{-3}$ M, it is clearly negligible showing how, at pH< 7, C18:0 sophorolipids quantitatively constitute the solid phase. This can be verified further. The second equivalence point at pH= 8.4 and V_{eq2}= 140 μL is also quite interesting as it corresponds to the titration of the solid fraction of C18:0 sophorolipids. The difference ΔV_{eq} (=V_{eq2}-V_{eq1}= 46 μL) corresponds then to the amount of NaOH used to titrate it, that is ~ $2.3 \cdot 10^{-3}$ M. Very interestingly, this amount is consistent with the initial concentration of C18:0 sophorolipids in solution ($1.6 \cdot 10^{-3}$ M). Thus, at pH= 8.5 practically the entire amount of C18:0 sophorolipids is titrated.

The pH-titration data can be compared with the DLS experiments. The superposition of the titration curve with the pH-dependent light scattering (Figure 3) shows the direct correlation between the protonation equilibrium starting between 9 < pH < 8 (empty triangles) and the initial formation of large aggregates for which an important light scattering phenomenon occurs (empty triangles). Superposition of the two experiments demonstrates the fact that the formation of large-scale assemblies starts below pH= 8.5 and that it is related with the protonation of the COOH group in C18:0 sophorolipids.

Characterization of the fibrillar ribbons. To characterize the self-assembly of C18:0 sophorolipids as a function of pH, we employed a combination of FE-SEM and high-resolution Cryo-TEM. According to SEM results, (Figure 4) the sample is constituted of a dense network of fibers, nicely showing the extent of the fibrillation process and the high level of entanglement at both pH= 2 and pH= 6 for the 5 mg/mL sample. Similar results are obtained at 2 mg/mL (images not shown). However, at pH= 11 (Figure 4D), one should note a radical change in the morphology, composed of round-shaped, sponge-like aggregates characterized by the absence of any fibrillar network. The self-assembly of C18:0 sophorolipids at this pH will not be discussed here but will be left for a future communication.

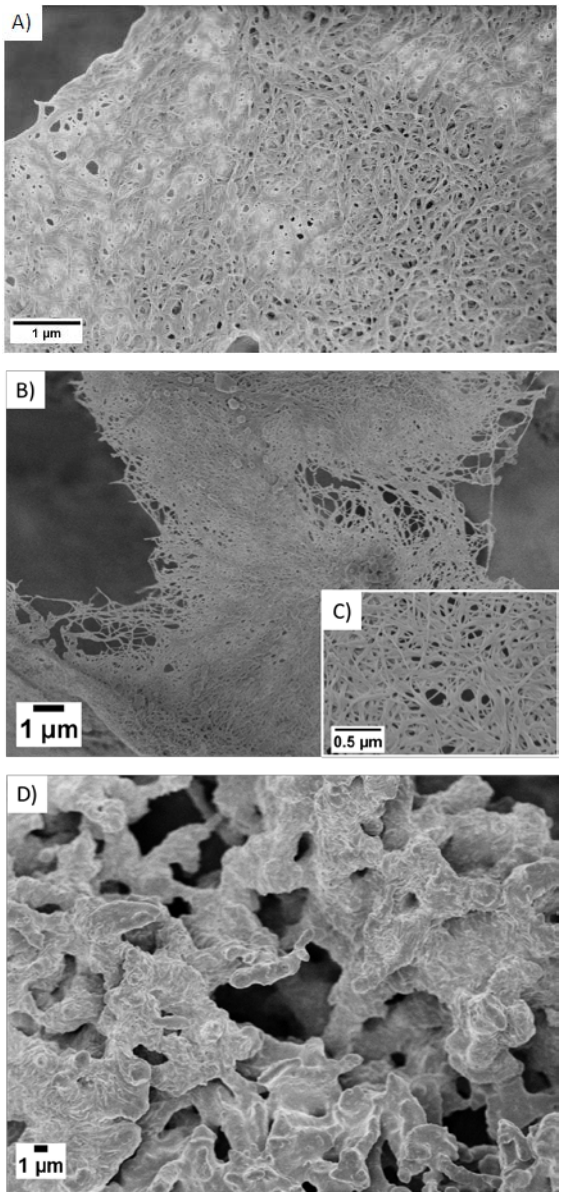

Figure 4 - FE-SEM images of C18:0 sophorolipids structures (c= 5 mg/mL) at (A) pH= 2, (B-C) pH= 6, (D) pH= 11

Cryo-TEM has been done on all samples to analyze the nature of the fibers. We report here the data taken on the 5 mg/mL sample at pH= 6 (Figure 5), while similar results are obtained for the pH=2 system. First of all, images A and B in Figure 5 show the presence of fibers with large aspect ratio, confirming the FE-SEM data. In addition, these images illustrate the presence of chirality at different scales: from single fibrils (Figure 5B, *Figure S3C*) up to associations of fibrils into thicker fibers. This specific point is highlighted by the arrows in Figure 5B and Figure 5C. In the former, we show various junction points where two or more fibrils form a larger fiber. Figure 5A shows a typical example of a large bundle composed of many individual fibrils.

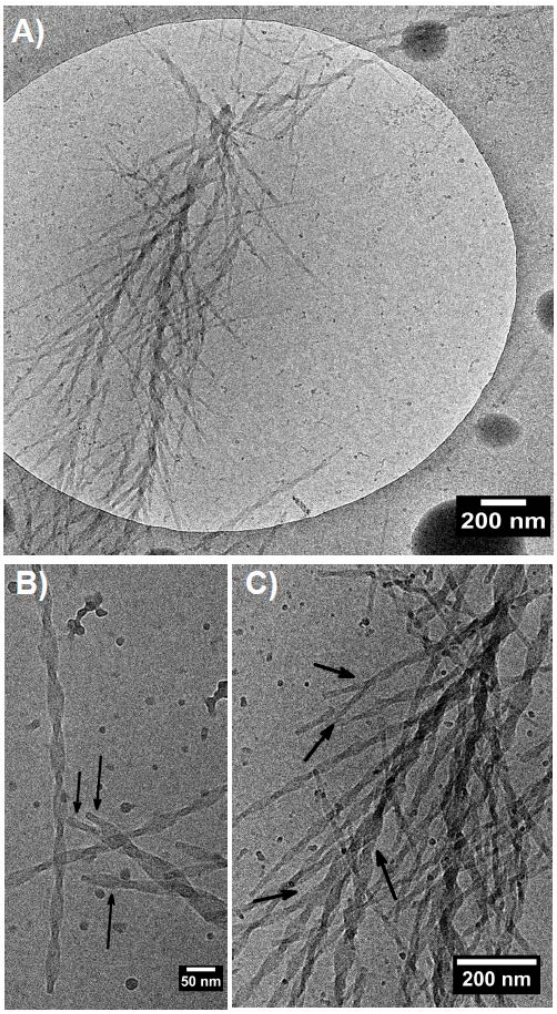

Figure 5 – (A-C) Cryo-TEM images of self-assembled C18:0 SL structures at 5 mg/mL, pH=6

Further images showing that chiral objects are ubiquitous are given in *Figure S3*A. The highlight in *Figure S3C* shows the dispersion in size of single fibrils (from about 10 nm to 25 nm) while Figure *S3B* further illustrates the entanglement between two fibrils into a larger one. Further proof ochirality is provided in *Figure S4A*, showing the shift of the ribbon pitches due to a tilt of the TEM grid, as indicated by the arrows.

Chiral fibers can either be twisted or helical and TEM is a common technique used to discriminate them. In this work, it seems that most objects are composed of left-handed twisted ribbons but we cannot exclude the presence of neither helical ribbons nor tubes. In the literature it was shown that time drives the formation

Table 1 - Summary of the overall dimensions measured for the chiral fibers formed by the self-assembly of C18:0 sophorolipids. Values in brackets refer to standard deviation.

pH	C (mg/mL)	Length (nm)	Pitch, *p* (nm)	Side width, *D* (nm)	*D/p*
2	2	200-310	206 (37)	18.5 (5.5)	0.09
	5	237-889	204 (42)	22.5 (10.5)	0.11
6	2	536-2100	171 (16)	17.5 (3.0)	0.10
	5	529-4200	241 (38)	33.5 (6.5)	0.14

of spherical particles that turn into twisted fibers then into helical and eventually nanotubes[35] and this effect cannot be excluded here. Ziserman *et al.*[34] have performed a statistical study on helical and twisted ribbons and could correlate the *D*/*p* ratio (where *D* is the side width of the ribbon and p is the pitch of the twist, *p*) with their abundance: $0.039 < D/p < 0.075$ for twisted structures (Class I) and $0.080 < D/p < 0.230$ for coiled/helical (Class II) ribbons.

On the basis of this particular classification we should expect both twisted and helical ribbons in our system, the typical dimensions of which are given in Table 1. The length of the ribbons at pH= 2 varies from 200 nm to 800 nm while *p* is about 205 nm, with a slightly higher dispersion for the 5 mg/mL system. *D* is about 20 nm but its dispersion in size can reach 50% for the 5 mg/mL concentration, as already commented in *Figure S3C*. Individual and highly entangled nanoribbons are found at pH= 6, reaching lengths as long as 2.1 µm (2 mg/mL) and 4.2 µm (5 mg/mL). *p*= 171 ± 16 nm for c= 2 mg/mL and *p*= 241 ± 38 nm for c= 5 mg/mL while *D* is, respectively, 17.5 ± 3.0 nm and 33.5 ± 6.5 nm. The difference in length between pH= 2 and pH= 6 could probably explain the DLS data in Figure 2A, that shows a decrease in diffused light from pH= 6 to pH= 2. However, variations in the fibrils' length is not specifically commented here because it can depend on many factors like maturation time, presence of salt, etc…

For the C18:0 sophorolipid, the estimated *D*/*p* (Table 1) are larger than 0.080, thus not excluding the presence of coiled/helical ribbons, even if mainly twisted ribbons are observed. This means that *D*/*p* values calculated here must be taken with caution as suggested by the large standard deviation in *p* and *D*.

At pH> 9, aggregates can still be seen but their shape is different and no chirality is detected, as also discussed below.

In fact, formation of chiral objects with pH can be monitored using circular dichroism (CD) even if it is well-known that CD is a delicate experiment with sugars[55] because they absorb light in the far-UV region. For this reason, we use it here in a qualitative way to present the optical activity of C18:0 sophorolipids with regard to pH (Figure 6). The spectra shows a flat background signal at basic pH, a sign that no chiral objects exist in solution. However, an optical activity occurs in the pH range corresponding to the formation of ribbons (pH 2 - 7), as seen by the broad CD signal at 210 nm. The positive dichroic band is probably related to the fact that sophorolipids are constituted of a di-glucose unit, with a C4 hydroxyl group in equatorial position, in agreement with previously reported data.[55]

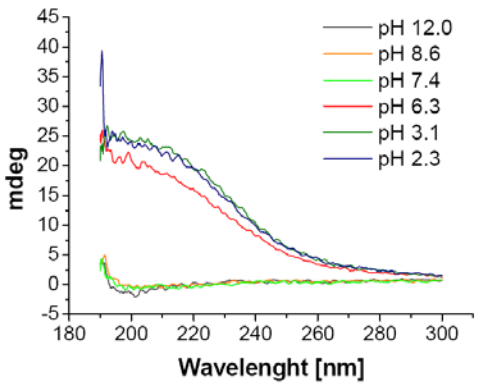

Figure 6 - Circular Dichroism spectra for a solution of C18:0 sophorolipid at a concentration of 5 mg/mL, room temperature and different pH values.

Conformational studies by SANS, WAXS and solid state NMR. The study of molecular conformation and packing within each ribbon has been done by a combination of SANS, WAXS and advanced two-dimensional ^{1}H-^{1}H solid state NMR spectroscopy.

Full squares in Figure 7a and b identify the SANS spectra for C18:0 sophorolipids at 5 mg/mL and pH= 6. At pH= 2, the SANS signature (not shown) is very similar to the one at pH= 6.

At this pH, the I(q) signal identifies at least three different zones : at q< 0.01 Å^{-1}, the intensity I(q)~ q^{-2}, which is a typical behavior observed for chiral ribbons, both theoretically[56] and experimentally;[57,49] at q > 0.01 Å^{-1}, the spectrum shows an inflection point where the variation of the characteristic slope is close to q^{-4}, typical for a sharp interface; for q > 0.10 Å^{-1}, an intense peak appears at about q= 0.237 Å^{-1}, corresponding to a periodic distance of d= 2.65 nm. Figure 7b shows the fit of the SANS spectrum using two functions, one using a model (lamellar form factor) function while the other is using a model independent (two-power law) function, where both functions display a I(q)~ q^{-2}xq^{-4} dependence, thus representing a good qualitative model for chiral ribbons.[56] As shown in Figure 7b, both functions nicely fit the data (please refer to *Section S.4* for the detailed parameters used in the fits), thus confirming the cryo-TEM experiments and suggesting that the sample is mostly composed of chiral ribbons.

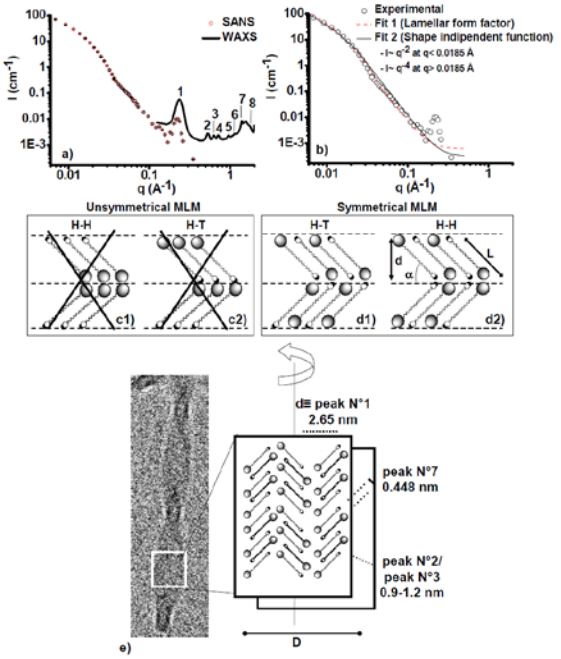

Figure 7 – (a) SANS (with error bars) and WAXS data recorded on the C18:0 sophorolipid at 5 mg/mL for pH= 6. (b) Qualitative fit of the SANS curve using a lamellar form factor and a model-independent two-power law (I~ q^{-2}q^{-4}) function implemented in the software SANSView. Parameters of the fit are given in *Section S.4*. (c,d) Monolayer Lipid Membrane (MLM) models adapted from ref. 58**. Unsymmetrical with (c1) Head-to-Head (H-H) and (c2) Head-to-Tail (H-T) polytypes. Symmetrical with (d1) H-T and (d2) H-H polytypes. (e) Scheme showing the possible molecular conformation within a ribbon of C18:0 sophorolipids at pH= 6. Peaks refer to WAXS data in (a).**

WAXS is extremely important to have an idea of the molecular packing within each ribbon. At pH= 6 (Figure 7a), the peak N°1 (q= 0.24 Å^{-1}) can be superimposed to the SANS peak mentioned above, but additional peaks (N°2 to N°8) are also detected. The full WAXS pattern and list of peaks are provided in *section S.8* (*Figure S5 and Table S1*).

Peak N°1 identifies the repeating inter-lipid layer distance within each ribbon, as largely discussed by Masuda[58] for similar, nanotube-forming, bola glycolipids. They have established an empirical relationship between d and L (the typical size of the glycolipid molecule, refer to Figure 7c,d) to describe the polymorph and polytype of the Monolayer Lipid Membrane (MLM). For the acidic C18:0 sophorolipids, L is not less than 3.8 nm,[1] which is larger than the d-values observed here (2.1-2.6 nm), and according to Masuda,[58] this leads to the hypothesis of an unsymmetrical MLM (Figure 7c). However, we exclude such hypothesis. In fact, the unsymmetrical MLM with H-H polytype (Figure 7c1) is excluded due to solid state NMR arguments, presented in more detail further below. The H-T polytype (Figure 7c2) is also excluded because a ribbons is characterized by a flat surface and a H-T polytype description is expected to give different chemical groups (sophorose vs. COOH) at each side of the ribbon. This is difficult to explain and it could be contradictory to the pH titration data, which show that the COOH group is only deprotonated at pH> 7, largely above its pKa value at equilibrium. The H-bonding network around

[1] Masuda et al calculate L to be about 3.38 nm for a similar C18:0 monosaccharide bola-glycolipid. To this value, one must add at least 0.5 nm to account for the second glucose in the C18:0 SL compound

the COOH probably protects it from water diffusion. For these reasons, we speculate that the lipid layer in the ribbons at pH= 6 rather adopts a bent symmetrical MLM conformation, as proposed in Figure 7d and where the difference between the H-T (Figure 7d1) and H-H (Figure 7d2) polytypes is not possible to make, yet. The bending angle, estimated to be $\alpha \sim 33°$, a value which is comparable with the one that has been reported by Masuda *et al*,[58] suggests an inter-layer packing in the ribbon plane , as shown in scheme in Figure 7. The close analysis of the full width at half maximum of peak N°1 contributes to such a picture. A rough estimation of the size of the crystallite from peak N°1 is about 13 nm (from the Scherrer formula), a value in the same order of magnitude as the side width, D, of the ribbons (Table 1). Similar arguments have been used before to associate the width of the XRD peak and molecular orientation in lipid-based ribbons.[59,38]

Abundant XRD data exist on twisted ribbons obtained from molecular systems and they help us in the tentative attribution of all other peaks in the WAXS spectrum. The interplanar distances found for peak N°2 (1.189 nm), peak N°3 (0.998 nm) and peak N°4 (0.880 nm) are very close, or even strictly equal, to the β-sheet (1.26-0.99 nm)[60,61,59] and inter-sheet (0.88 nm)[62] stacking in chiral self-assembled peptides and amyloid. The value for peak N°7 (0.448 nm) is very close to 0.475 ± 0.001 nm, generally attributed to the interstrand H-bonding distance.[62,61] The scheme in Figure 7e fits the literature data for the C18:0 sophorolipid system. WAXS data showing an inter-sheet stacking of fibrils, like in the amyloid fiber system, is also confirmed by the previously presented bundles in the cryo-TEM images. Finally, the mild but appreciable shoulder at d= 0.36 nm (peak N°8, only seen at pH= 6) is very close to the reflection at d= 0.39 nm, apparently very specific of a chiral superstructure, according to Castelletto *et al*.[59]

The symmetrical polymorph conformation, which can only be supposed by XRD arguments, can be proved by 2D ^{1}H-^{1}H solid state MAS NMR spectroscopy using the BABA pulse sequences (presented in *section S.4*) and ^{1}H-^{13}C 2D heteronuclear correlation spectroscopy (see *section S.9*).

These techniques probe through-space ^{1}H-^{1}H (< 5 Å) and ^{13}C-^{1}H proximities using the nuclear spin interactions (dipolar coupling).

The ^{1}H fast MAS NMR spectra of the freeze dried powders at pH= 6 is given in Figure 8A. Despite the very fast MAS rate (65 kHz), the signal is still quite broad, which can come from both the strong coupling between protons and dispersion in chemical shifts typical for solid state spectra. However, one can safely assign (detailed assignment of ^{1}H NMR peaks is done in *Figure S1*) the peak at: δ= 1.3 ppm to the aliphatic protons (a: -$(CH_2)_n$-), δ= 3.8 ppm to the sophorose protons (b: $H'_{2\text{-}6}$; $H''_{2\text{-}6}$), δ= 4.8 ppm to water (c), δ~ 5.6 ppm to COO<u>H</u> (d). The COOH group, characterized by an unshielded broad hump expected for labile protons in hydrogen bonding, is only detected for the chiral ribbons at pH= 6, for which protonation occurs. Only the water signal is detected at pH= 11, the reason for which the corresponding spectrum has been represented. The double-quantum single quantum 2D ^{1}H-^{1}H MAS NMR experiment (Figure 8B) provides a direct view of the intermolecular interactions: on-diagonal (a) and (b) and off-diagonal (a-b) cross peaks show, respectively, the trivial intra-aliphatic (a-a), intra-sophorose (b-b) and aliphatic-sophorose (a-b) interactions. Even if it is not possible to be more precise on which specific hydrogen of these groups is concerned by the interactions, the off-diagonal cross-peaks (b-d) (Figure 8B) provide the direct proof of the hydrogen bonding between COOH and sophorose (Figure 8C). The proximity between them is also largely confirmed by 2D ^{13}C-^{1}H HETCOR MAS NMR spectroscopy (*Figure S9*) performed on both dried and wet gels composed of chiral ribbons. This is largely commented in *section S.4*.

Our extensive solid state NMR analysis strongly suggests the adoption of the symmetrical polymorph, probably in the H-T conformation (Figure 7d1).

However, a weak on-diagonal (d-d) cross-peak in Figure 8B should also be considered and it may suggest hydrogen bonding between two close COOH groups (Figure 8C), thus not excluding the presence of a H-H polytype (Figure 7d2).

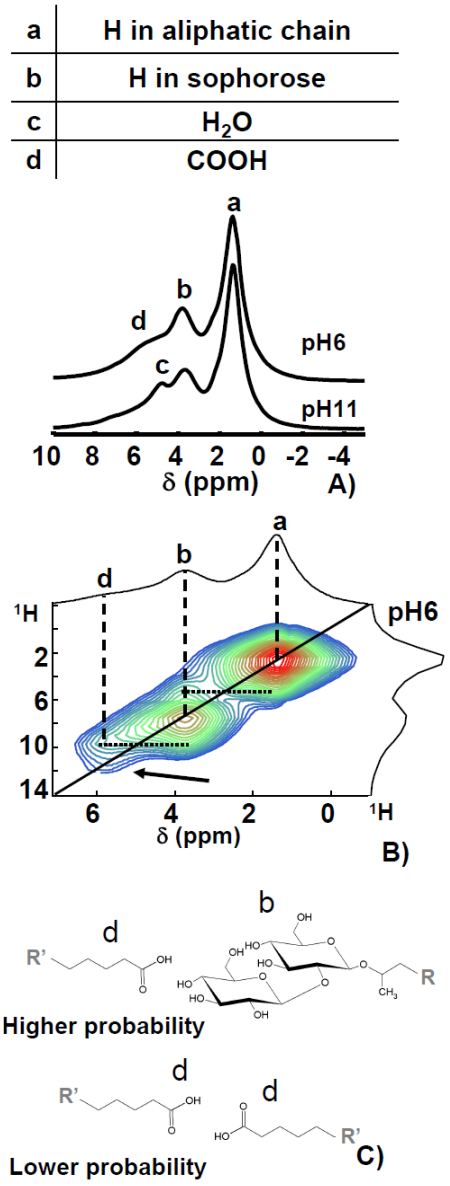

Figure 8 – (A) ^{1}H MAS NMR spectra recorded on the C18:0 sophorolipid at 5 mg/mL and at pH= 6 and pH= 11. 2D ^{1}H-^{1}H MAS NMR maps obtained at (B) pH= 6 using the double-quantum single-quantum excitation-reconversion BABA pulse sequence. (C) Local molecular conformation deduced from solid state NMR at pH= 6.

Discussion

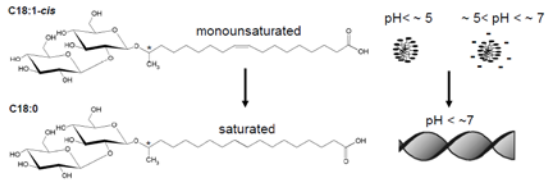

Scheme 1 – Summary of the differences in the self-assembly behaviour between the C18 :1-*cis* and C18 :0 sophorolipids at pH< ~7 at the same temperature and time scale. Data on the C18 :1-*cis* sophorolipid can be found in ref. [53,52] The asterisk identifies the chiral subterminal carbon. The image of the ribbon has been adapted from ref. [16] (Copyright © 1999, Nature Publishing Group).

Scheme 1 summarizes the nature of self-assembled structures found on both the C18:1-*cis* and C18:0 sophorolipids at neutral/acidic pH processed under the same conditions. The monounsaturated compound forms micelles, whose charge can be tuned with pH,[52,53] while the saturated compound (refer also to Table 2, sample 9) immediately forms nanoscale ribbons with supramolecular chirality. This structure, at such scales, has not been observed before for any other sophorolipid. Prasad *et al*.[51] suggested that the bulky sophorose group could be responsible for the formation of giant micronic ribbons for the C18:1-*trans* sophorolipid. However, they reported the formation of flat sheets for the C18:0 sophorolipid (sample 9 in Table 2), which also has an elongated conformation of the aliphatic chain. In the literature, some key chemical groups seem to promote chirality in glycolipids at the nanoscale. As shown in Table 2, non-bola compounds (e.g., samples 1 to 4) need an interaction-promoting (hydrogen bonding, π-π stacking)[63,64] linker (phenyl, phenylamide, amidopyridine) rather than specific saturation/unsaturation ratios. For instance, ether linkers only promote micelles but never lead to the formation of fibers (compound N°7 in Table 2). Asymmetric bolas close to C18:0 sophorolipids, like compound 8 in Table 2, always form nanotubes, despite the type of linker. The nature of the sugar may have some important influence on the extent of hydrogen bonding network. For instance, the axial orientation of the C_4-OH in galactose promotes a 3D network while the planar C_4-OH configuration in glucose is responsible for a 2D structure.[65] The

influence of the type of sugar on the type of fiber was largely documented by Frankel[63]. Solvent (mixtures) or heating/cooling cycles generally promote the formation of chiral fibers.

According to these considerations, the C18:0 sophorolipid may not be expected to form chiral fibers in water at room temperature even if the presence of two glucose units may have some unexpected effects. However, this cannot fully explain the origin of chirality. As discussed in the introduction, supramolecular chirality is often induced by local stereocenters. In this sense, the C18:0 sophorolipid is quite interesting. The ether bond linker between sophorose and stearic acid occurs on the C_{17} in a 95/5 ratio with respect to C_{18}. This is well-known from the biosynthesis of sophorolipids by the yeast *Starmerella bombicola*.[66] Terminal (C_{18}) hydroxylation has no influence on chirality, but the subterminal (C_{17}) is always in the *S*-enantiomeric form. [2] It is highly possible that the chiral C_{17} atom plays an important role in the formation of the nanoscale ribbons, but additional driving forces must contribute to this process. First of all, chirality in the C18:0 sophorolipid system is a hydrogen-bond driven mechanism (proofs by pH-titration, DLS and solid state NMR).

Furthermore, parallel experiments run on the C18:1-*cis* sophorolipids do not show the formation of any chiral supramolecular structure under acidic pH conditions neither on the same time scale nor at longer reaction times. This is shown in Figure 2 and largely discussed in ref. [52] (refer also to Scheme 1) The effect of time reported by us[53] and by others[50] is still not clear and deserves further investigation. In the end, both hydrophobic interactions and hydrogen bonding, besides the stereocenter located on C_{17}, play a major role in the stabilization of the supramolecular chiral ribbons. These facts are started to be unraveled only recently on well-designed compounds. For instance, Ziserman *et al*.[35] discussed the fact that these three conditions must be fulfilled at the same time for an engineered lysine-based amphiphile containing a double C_{12} aliphatic chain. In their case, they could demonstrate that supramolecular chirality was driven by the hydrophobic packing of the bent C_{12} chains and side H-bonding interactions between the lysine groups, which also contain a stereocenter. For the actual mechanism of chirality transfer from a molecular to a supramolecular level, Oda *et al.*[38] have commented that twisting is necessary to release local tensions, which were due in their case to the constraint issued by the angle between the chiral tartrate anion and the ribbon longest axis (about 38°). In the model presented in Figure 7d for C18:0 sophorolipids, the molecules experience a 33° angle with respect to the ribbon major axis and twisting could result from such a torsion.

The formation of a symmetrical MLM (Figure 7d) could also induce a high concentration of sophorose groups inside the ribbon plane. The combination of all these parameters could then justify the formation of supramolecular chirality to release local tensions.

Another unclear issue is the lack of rapid supramolecular chirality for the C18:1-*cis* sophorolipid. Even if this system was reported to form giant ribbons (but never nanoscale ones),[50] we found them difficult to reproduce. The work of Prasad *et al*. also seem to go in this sense, as they only obtained giant ribbons with a clear CD signature for the C18:-*trans* sophorolipids.[51] One could argue that the presence of a *cis* double bond plays against a tight molecular packing. However, saturation was shown to be one of the chiral-forming elements in several non-bola compounds (samples 1 to 5 in Table 2). In the C18:1-*cis* sophorolipid, it may occur that packing between the C18:1 chains needs longer stabilization times and/or that the double bond helps releasing more easily the local tensions that seem necessary to induce chirality. This question is still unanswered.

[2] The IUPAC name for sophorolipids is: 17-L-([2-O-β-D-glucopyranosyl-β-D-glucopyranosyl]-oxy)-octadecenoic acid

Table 2 – Morphological variation of representative glycolipids in the literature according to the nature of the sugar (A), linker (B), *cis*-double bond (C) and end-group (D), as schematized in the image on the right hand side.

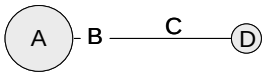

Sample	A (sugar)	B (linker)	C (*cis*-double bonds)	D (end-group)	Morphology	Ref
1	glucose	phenyl	yes	CH_3	chiral fibers	15
2	glucose	phenyl	no	CH_3	chiral fibers	15
3	glucose	phenylamide	yes	CH_3	chiral fibers	47
4	glucose	phenylamide	no	CH_3	fibers	47
5	glycoside	amidopyridine	yes	CH_3	chiral fibers nanotubes	48
6	glycoside	amidopyridine	no	CH_3	fibers	48
7	glucose	ether	no	CH_3	clear solution	15
8	glucose	amide	no	COOH	nanotubes	24
9	sophorose	ether	no	COOH	chiral fibers @ pH< 7.5	This work
″	″	″	″	″	flat sheets	51

Conclusion. This work shows how supramolecular nanoscale chirality can be obtained from yeast-derived asymmetric bola-glycolipids and how such a phenomenon is strongly related to the coexistence of several "chirality triggers": stereocenters, hydrogen bonding, hydrophobic interactions and, above all, pH. This work also illustrates that such behaviour is still difficult to predict, at least for bolaform glycolipids, and still needs to be studied in a systematic way as it has been done for aminoacid and peptide-based amphiphiles.

Acknowledgements : The research leading to these results has received funding from the European Community's Seventh Framework Programme (FP7/2007-2013) under Grant Agreement n° Biosurfing/289219. Patrick Le Griel and Gervaise Mosser (LCMCP, Collège de France, Paris, France) are acknowledged for their help on cryo-TEM. Sophie Cassaignon, Guillaume Laurent and Carole Aimé (LCMCP, Collège de France, Paris, France) are warmly acknowledged for their help and helpful discussion on, respectively, pH titration, solid state NMR and circular dichroism. David Montero and Cristina Coelho-Diogo (Institut des Matériaux de Paris Centre, Paris, France) have kindly provided their help for FE-SEM and solid state NMR (Bruker AV700) experiments.

References

1. D. Philp and J. F. Stoddart, *Angew. Chem. Int. Ed. Engl.*, 1996, **35**, 1154–1196.
2. M. R. Falvo, S. Washburn, R. Superfine, M. Finch, F. P. Brooks, V. Chi, and R. M. Taylor, *Biophys. J.*, 1997, **72**, 1396–1403.
3. J. F. Smith, T. P. J. Knowles, C. M. Dobson, C. E. Macphee, and M. E. Welland, *Proc. Nat. Ac. Sci. USA*, 2006, **103**, 15806–15811.
4. M. R. Sawaya, S. Sambashivan, R. Nelson, M. I. Ivanova, S. a Sievers, M. I. Apostol, M. J. Thompson, M. Balbirnie, J. J. W. Wiltzius, H. T. McFarlane, A. Ø. Madsen, C. Riekel, and D. Eisenberg, *Nature*, 2007, **447**, 453–457.
5. R. Nelson, M. R. Sawaya, M. Balbirnie, A. Ø. Madsen, C. Riekel, R. Grothe, and D. Eisenberg, *Nature*, 2005, **435**, 773–778.
6. A. Gautieri, S. Vesentini, A. Redaelli, and M. J. Buehler, *Nano Lett.*, 2011, **11**, 757–766.
7. L. Hsu, G. L. Cvetanovich, and S. I. Stupp, *J. Am. Chem. Soc.*, 2008, **130**, 3892–2899.
8. J. C. Stendahl, M. S. Rao, M. O. Guler, and S. I. Stupp, *Adv. Funct. Mater.*, 2006, **16**, 499–508.
9. R. M. Capito, H. S. Azevedo, Y. S. Velichko, A. Mata, and S. I. Stupp, *Science*, 2008, **319**, 1812–1816.
10. J. D. Hartgerink, E. Beniash, and S. I. Stupp, *Science*, 2001, **294**, 1684–1688.
11. V. M. Tysseling-Mattiace, V. Sahni, K. L. Niece, D. Birch, C. Czeisler, M. G. Fehlings, S. I. Stupp, and J. a Kessler, *J. Neurosci.*, 2008, **28**, 3814–23.
12. R. N. Shah, N. a Shah, M. M. Del Rosario Lim, C. Hsieh, G. Nuber, and S. I. Stupp, *Proc. Nat. Ac. Sci. USA*, 2010, **107**, 3293–3298.
13. A. Mata, Y. Geng, K. J. Henrikson, C. Aparicio, S. R. Stock, R. L. Satcher, and S. I. Stupp, *Biomaterials*, 2010, **31**, 6004–6012.
14. A. Aggeli, I. A. Nyrkova, M. Bell, R. Harding, L. Carrick, T. C. B. Mcleish, A. N. Semenov, and N. Boden, *Proc. Nat. Ac. Sci. USA*, 2001, **98**, 11857–11862.
15. G. John, M. Masuda, Y. Okada, K. Yase, and T. Shimizu, *Adv. Mater.*, 2001, **13**, 715–718.
16. R. Oda, I. Huc, M. Schmutz, S. J. Candau, and F. C. MacKintosh, *Nature*, 1999, **399**, 566–569.
17. J. Schneider, C. Messerschmidt, A. Schulz, M. Gnade, B. Schade, P. Luger, P. Bombicz, V. Hubert, and J.-H. Fuhrhop, *Langmuir*, 2000, **16**, 8575–8584.
18. T. Wang, J. Jiang, Y. Liu, Z. Li, and M. Liu, *Langmuir*, 2010, **26**, 18694–18700.
19. Y. Zhou, M. Kogiso, M. Asakawa, S. Dong, R. Kiyama, and T. Shimizu, *Adv. Mater.*, 2009, **21**, 1742–1745.

20. V. Dinca, E. Kasotakis, J. Catherine, A. Mourka, A. Ranella, A. Ovsianikov, B. N. Chichkov, M. Farsari, A. Mitraki, and C. Fotakis, *Nano Lett.*, 2008, **8**, 538–543.
21. M. Reches and E. Gazit, *Science*, 2003, **300**, 625–627.
22. E. Gazit, *Chem. Soc. Rev.*, 2007, **36**, 1263–1269.
23. T. Shimizu, *J. Polym. Sci. Part A*, 2008, **46**, 2601–2611.
24. N. Kameta, H. Minamikawa, and M. Masuda, *Soft Matter*, 2011, **7**, 4539–4561.
25. P. Terech, S. Friol, N. Sangeetha, Y. Talmon, and U. Maitra, *Rheol. Acta*, 2006, **45**, 435–443.
26. T. Toksoz and M. O. Guler, *Nano Today*, 2009, **4**, 458–469.
27. M. S. Lamm, N. Sharma, K. Rajagopal, F. L. Beyer, J. P. Schneider, and D. J. Pochan, *Adv. Mater.*, 2008, **20**, 447–451.
28. H. Moshe, M. Vanbel, V. K. Valev, T. Verbiest, D. Dressler, and Y. Mastai, *Chemistry, Europ. J.*, 2013, **19**, 10295–10301.
29. Z. Qi, C. Wu, P. Malo de Molina, H. Sun, A. Schulz, C. Griesinger, M. Gradzielski, R. Haag, M. B. Ansorge-Schumacher, and C. a Schalley, *Chemistry, Europ. J.*, 2013, **19**, 10150–10159.
30. O.-Y. Zhong-can, S. Liu, and X. Yu-Zhang, *Phys. Rev. Lett.*, 1990, **64**, 1679.
31. J. V. Selinger, F. C. MacKintosh, and J. M. Schnur, *Phys. Rev. E*, 1996, **53**, 3804–3818.
32. P.-G. de Gennes, *C. R. Acad. Sci. Paris*, 1987, **304**, 259.
33. R. Selinger, J. Selinger, A. Malanoski, and J. Schnur, *Phys. Rev. Lett.*, 2004, **93**, 158103.
34. L. Ziserman, A. Mor, D. Harries, and D. Danino, *Phys. Rev. Lett.*, 2011, **106**, 238105.
35. L. Ziserman, H.-Y. Lee, S. R. Raghavan, A. Mor, and D. Danino, *J. Am. Chem. Soc.*, 2011, **133**, 2511–2517.
36. R. Oda, F. Artzner, M. Laguerre, and I. Huc, *J. Am. Chem. Soc.*, 2008, **130**, 14705–14712.
37. H. Cao, X. Zhu, and M. Liu, *Angew. Chem. Int. Ed. Engl.*, 2013, **52**, 4122–4126.
38. A. Brizard, C. Aimé, T. Labrot, I. Huc, D. Berthier, F. Artzner, B. Desbat, and R. Oda, *J. Am. Chem. Soc.*, 2007, **129**, 3754–3762.
39. W. Von Rybinski and K. Hill, *Angew. Chem. Int. Ed. Engl.*, 1998, **37**, 1328–1345.
40. D. C. Kennedy, D. Grünstein, C.-H. Lai, and P. H. Seeberger, *Chemistry, Europ. J.*, 2013, **19**, 3794–3800.
41. J. Axford, *Trends Immunol.*, 2001, **22**, 237–239.
42. T. Shimizu, *Bull. Chem. Soc. Jap.*, 2008, **81**, 1554–1566.
43. J. D. Desai and I. M. Banat, *Microbiol. Molec. Biol. Rev.*, 1997, **61**, 47–64.
44. I. M. Banat, R. S. Makkar, and S. S. Cameotra, *Appl. Microbiol. Biotechnol.*, 2000, **53**, 495–508.
45. Y. Lin, Y. Qiao, P. Tang, Z. Li, and J. Huang, *Soft Matter*, 2011, **7**, 2762–2769.
46. N. Kameta, M. Masuda, and H. Minamikawa, *Langmuir*, 2007, **23**, 4634–4641.
47. S. Kamiya, H. Minamikawa, J. H. Jung, B. Yang, M. Masuda, and T. Shimizu, *Langmuir*, 2005, **21**, 743–750.
48. G. John, M. Mason, P. M. Ajayan, and J. S. Dordick, *J. Am. Chem. Soc.*, 2004, **126**, 15012–15013.
49. H. Cui, T. Muraoka, A. G. Cheetham, and S. I. Stupp, *Nano Lett.*, 2009, **9**, 945–951.
50. S. Zhou, C. Xu, J. Wang, W. Gao, R. Akhverdiyeva, V. Shah, and R. Gross, *Langmuir*, 2004, **20**, 7926–7932.
51. P. Dhasaiyan, A. Banerjee, N. Visaveliya, and B. L. V Prasad, *Chemistry, Asian J.*, 2013, **8**, 369–372.
52. N. Baccile, F. Babonneau, J. Jestin, G. Pehau-Arnaudet, and I. Van Bogaert, *ACS Nano*, 2012, **6**, 4763–4776.
53. N. Baccile, J. S. Pedersen, G. Pehau-Arnaudet, and I. N. a. Van Bogaert, *Soft Matter*, 2013, **9**, 4911–4922.
54. T. Shimizu, M. Masuda, and H. Minamikawa, *Chem. Rev.*, 2005, **105**, 1401–1443.
55. R. G. Nelson and W. C. Johnson, *J. Am. Chem. Soc.*, 1971, **53**, 3343–3345.
56. I. W. Hamley, *Macromolecules*, 2008, **41**, 8948–8950.
57. J. E. Goldberger, E. J. Berns, R. Bitton, C. J. Newcomb, and S. I. Stupp, *Angew. Chem. Int. Ed. Engl.*, 2011, **50**, 6292–6295.
58. M. Masuda and T. Shimizu, *Langmuir*, 2004, **20**, 5969–5977.
59. V. Castelletto, I. W. Hamley, R. a Hule, and D. Pochan, *Angew. Chem. Int. Ed. Engl.*, 2009, **48**, 2317–2320.
60. A. K. Mehta, K. Lu, W. S. Childers, Y. Liang, S. N. Dublin, J. Dong, J. P. Snyder, S. V. Pingali, P. Thiyagarajan, and D. G. Lynn, *J. Am. Chem. Soc.*, 2008, **130**, 9829–9835.
61. E. T. Pashuck and S. I. Stupp, *J. Am. Chem. Soc.*, 2010, **132**, 8819–8821.
62. A. M. Squires, G. L. Devlin, S. L. Gras, A. K. Tickler, C. E. MacPhee, and C. M. Dobson, *J. Am. Chem. Soc.*, 2006, **128**, 11738–11739.
63. D. A. Frankel and D. F. O'Brien, *J. Am. Chem. Soc.*, 1994, **116**, 10057–10069.
64. J. H. Jung, G. John, K. Yoshida, and T. Shimizu, *J. Am. Chem. Soc.*, 2002, **124**, 10674–10675.
65. M. Masuda and T. Shimizu, *Carbohyd. Res.*, 2000, **326**, 56–66.
66. I. N. a Van Bogaert, J. Sabirova, D. Develter, W. Soetaert, and E. J. Vandamme, *FEMS yeast research*, 2009, **9**, 610–7.